

VДК 537.591.15

## POSSIBILITY TO DETECT COSMIC PARTICLES AND NEUTRINO OF SUPER-HIGH ENERGIES IN ATMOSPHERIC AIR AND CONDENSED MEDIA USING MAGNETOINDUCTIVE METHOD

**V.M. Kartashev, V.E. Kovtun, O.K. Minko, Yu.P. Poltoratskaya, E.S. Shmatko, I.I. Zaliubovskii**

*The V.N. Karazin Kharkov National University, Kharkov, Ukraine*

Received April 20, 2004

A possibility was considered to detect cosmic particles and neutrinos of super-high energies using the electromagnetic induction of the excess electrons in an extensive air shower (EAS) as well as in showers occurring in condensed media (ice, halite). Electromagnetic induction caused by the showers occurring in the mentioned media was calculated. The structure of a detector based on this principle has been offered. The detector response was calculated for different distances from the shower axis. The detector energy threshold was estimated to be  $\sim 10^{12}$  eV for the showers in condensed media, and  $\sim 10^{16}$  for the EAS.

**KEY WORDS:** extensive air shower, excess electrons, electromagnetic induction shower, induction detector.

The galactic sources of cosmic charged particles and neutrinos of super-high energies are the same astrophysical objects. Supernovas and their remnants (pulsars) are the most powerful of them. Charged particles are accelerated within the shells of Supernovas and in the immediate environment of the pulsars. Neutrinos are, mainly, decay products of  $\pi$ - and K-mesons. The latter are born in nuclear interactions of the accelerated charged particles with the medium ambient to the mentioned objects. Dispersed background of such neutrinos that are born under the influence of cosmic rays in the atmospheres of stars and planets, as well as in the intensive Galactic light fluxes also occurs. Cosmic particles of super-high energies in the Earth atmosphere give rise to extensive air showers by which they are detected. Neutrinos of super-high energies ( $>10^{11}$  eV) in thick layers of the medium interact via a stage of vector W-bosons birth, which when decaying into hadrons and leptons are forming electron-photon showers as well. Unlike their characteristics in the air, in the dense medium the showers have short periods of their development and transverse dimensions. Therefore, in order to enlarge the effective detection area a technique is required to detect these showers at a large distance from their axis. The showers in condensed transparent medium are generally detected by their Cerenkov optical radiation.

This paper suggests detection of extensive air showers in the air and electron-photon showers in condensed medium by magnetic induction of their excess electrons. The latter are formed in three elementary processes: annihilation of shower positrons and the medium electrons when they are in flight; scattering of shower positrons and electrons on the medium electrons and consequent generation of  $\delta$ -electrons; Compton electron generation caused by the shower photon scattering on the medium electrons. Askar'yan G.A., a physicist from Moscow, was the first to estimate the shower excess electrons [1].

### DIFFERENTIAL ENERGY SPECTRUM OF EXCESS ELECTRONS OF ELECTRON-PHOTON SHOWERS IN VARIOUS MEDIA

The calculation of excess electron differential energy spectrum as well as magnetic induction in the extensive air showers (EAS) and in electron-photon showers originating in the condensed media was grounded on simulation of their development process with using simplified approximation formulas for the shower theory. The procedure like this allows simplifying rather intricate calculations without essential sacrifice of accuracy.

#### Energy spectra of charged particles and photons in the shower maximum development

The equilibrium Tamm-Belenky integral energy spectrum of shower electrons has been assumed as the basic one [2]. From it the equilibrium integral energy spectrum of shower photons was derived [3]. Both equilibrium spectra are of the same form as the spectra of particles and photons in the maximum shower development. Electron differential spectrum approximation in the maximum shower development was derived from [4]:

$$\varphi_e^{\max}(E)dE = \frac{2.29}{E_{cr}} \cdot \frac{dE}{\left(1 + \frac{2.29}{E_{cr}} E\right)^2} \quad (1)$$

Spectrum (1) was normalized so, that  $\int_0^{\infty} \varphi_e^{\max}(E)dE = 1$ . In formula (1) E is kinetic energy of shower electrons, MeV;

$E_{cr}$  – critical energy of shower particles in a selected medium. Spectrum (1) can be applied for extensive air showers at the sea level too since its effective age at relatively small distances from the axis remains near one (what corresponds to

the shower development maximum) in the wide range of development depths due to its replenishment by the nuclear-cascade process. Relying on the spectrum (1) and on the interconnection between the integral energy spectra of electrons and photons that was obtained from the shower theory [3], the authors suggested the approximation of the photon differential energy spectrum in the shower maximum development in the form [5]:

$$\varphi_{\gamma}^{\max}(E_{\gamma})dE_{\gamma} = \frac{2.29}{E_{cr}} \left\{ \frac{2\varepsilon^3 - 2\varepsilon^2 [2 \ln(0.3679 + \varepsilon) - 1.3679] - \varepsilon [1.4715 \cdot \ln(0.3679 + \varepsilon) + 3] + 1.8964}{3\mu_0(0.3679 + \varepsilon)(1 + 0.6667\varepsilon^2)^2} \right\} dE_{\gamma}. \quad (2)$$

Here  $\varepsilon = 2.29E_{\gamma}/E_{cr}$ ;  $E_{\gamma}$  – photon energy, MeV;  $\mu_0 \approx 0.7$  – coefficient of photon absorption in light matters at high energies, calculated for one radiation length [3].

Total number of charged particles at all the energies for light enough substances in the shower maximum development is described by a simple expression [3]:

$$N_{\max} = \frac{0.31}{\sqrt{\ln\left(\frac{E_0}{E_{cr}}\right)}} \cdot \frac{E_0}{E_{cr}}, \quad (3)$$

where  $E_0$  – energy of the primary electron or photon that caused the shower ( $E_0 \gg E_{cr}$ ).

For extensive air showers expression (3) is non-applicable since they are detected on the Earth surface (at the sea level) and not in their maximum development, and they are superposition of a number of partial showers produced by  $\gamma$ -quanta. Therefore the number of EAS particles was calculated by transforming the empirical formula that was derived during investigations carried out on the Yakutsk EAS array [6]:

$$E_0 = (7.7 \pm 2.5) 10^{17} \left( \frac{N}{10^8} \right)^{0.86 \pm 0.06}, \quad (4)$$

where  $E_0$  – cosmic particle primary energy in eV,  $N$  – total number of the EAS particles near the sea level.

#### Shower electron excess caused by positron annihilation in flight

Annihilation of shower positron in flight occurs both with bound medium electrons and with free ones. The residuary shower excess electrons have the same energy spectrum as positrons absorbed in the process of annihilation. Total effective annihilation cross-sections, as energy functions of on-flying positrons, are universal for any medium and depend only upon the number of Z-electrons contained in a neutral atom [7]:

$$\sigma_{an1} = 4\pi Z^5 \alpha^4 r_0^2 \frac{1}{(\gamma_+ + 1)^2 \sqrt{\gamma_+^2 - 1}} \left[ \gamma_+^2 + \frac{2}{3}\gamma_+ + \frac{4}{3} - \frac{\gamma_+ + 2}{\sqrt{\gamma_+^2 - 1}} \ln(\gamma_+ + \sqrt{\gamma_+^2 - 1}) \right], \quad (5)$$

$$\sigma_{an2} = \pi Z r_0^2 \frac{1}{\gamma_+ + 1} \left[ \frac{\gamma_+^2 + 4\gamma_+ + 1}{\gamma_+^2 - 1} \ln(\gamma_+ + \sqrt{\gamma_+^2 - 1}) - \frac{\gamma_+ + 3}{\sqrt{\gamma_+^2 - 1}} \right]. \quad (6)$$

Here indices "an1" и "an2" are for the bound electrons and the free ones, accordingly. The other symbols are:  $\alpha = 1/137$  – the fine structure constant,  $r_0 = 2.8175 \cdot 10^{-13}$  cm – the electron classic radius,  $\gamma_+ = (E_+ + mc^2)/mc^2$  – on-flying positron Lorentz factor,  $mc^2 = 0.511$  MeV – the electron (positron) rest energy. Minimal positron energy was assumed to be 1 MeV.

#### Ice (fresh water)

Differential energy spectrum of excess electrons in the process of annihilation is written as follows:

$$N_{an}^{ice}(E)dE = 0.5 N_{\max} n_{ice} \Delta x_{ice} \left\{ \left[ 2\sigma_{an1}^H(E) + \sigma_{an1}^0(E) \right] + \left[ 2\sigma_{an2}^H + \sigma_{an2}^0(E) \right] \right\} \varphi_e^{\max}(E)dE. \quad (7)$$

The symbols in (7) denote the following:  $n_{ice} = 3.065 \cdot 10^{22}$  cm<sup>-3</sup> – concentration of water molecules in the ice;  $\Delta x_{ice} = 0.12E / \{\rho_{ice}(dE/dx)_{total}\}$  cm – ice layer thickness for single collisions (1/5 of the positron free path average length with respect to interactions of all kinds);  $\rho_{ice} = 0.917$  g/cm<sup>3</sup> – ice density;  $(dE/dx)_{total}$  – total specific positron energy losses, MeV·cm<sup>2</sup>/g (tabulated or calculated values);  $E_{cr} = 73$  MeV;

#### Air (75.5% N<sub>2</sub> + 23.15% O<sub>2</sub> + 1.292% Ar + 0.046% CO<sub>2</sub> + 0.012% (Ne, etc.) in mass)

$$N_{an}^{air}(E)dE = 0.5 N n_{air} \Delta x_{air} \left\{ \sigma_{an1}^{air}(E) + \sigma_{an2}^{air}(E) \right\} \varphi_e^{\max}(E)dE. \quad (8)$$

Here  $n_{air}=5.0 \cdot 10^{19} \text{ cm}^{-3}$  – effective concentration of conditional air molecules at the sea level;  $\Delta x_{air}=0.12E/\{\rho_{air} (dE/dx)_{total}\} \text{ cm}$  – air layer thickness for single collisions;  $\rho_{air}=1.205 \cdot 10^{-3} \text{ g/cm}^3$  (1 atm., 20°C);  $Z_{air}=7.233$  – effective ordinal number of the conditional air atom;  $E_{cr}=81 \text{ MeV}$ ;  $N$  is defined from (4) at the selected energy of the primary cosmic particle  $E_0$ .

#### Halite (NaCl)

$$N_{an}^{NaCl}(E)dE = 0.5N_{max}n_{NaCl}\Delta x_{NaCl}\left\{\sigma_{an1}^{Na}(E) + \sigma_{an2}^{Na}(E) + \sigma_{an1}^{Cl}(E) + \sigma_{an2}^{Cl}(E)\right\}\varphi_e^{\max}(E)dE. \quad (9)$$

Here  $n_{NaCl}=2.231 \cdot 10^{22} \text{ cm}^{-3}$ ;  $\Delta x_{NaCl}=0.12E/\{\rho_{NaCl}(dE/dx)_{total}\} \text{ cm}$ ;  $\rho_{NaCl}=2.165 \text{ g/cm}^3$ ;  $E_{cr}=36.2 \text{ MeV}$ . Table of symbols is the same as in (7).

#### $\delta$ -Electron excess caused by shower positron scattering on atomic electrons

Here only scattering of positrons, having kinetic energy  $E_+ \geq 1 \text{ MeV}$ , is considered for the following reasons: only the electron whose energy after the process of scattering is higher remains in the shower at low energies which happens owing to the identity of shower electrons and medium electrons. This situation does not result in forming of the electron excess. On the contrary, positron scattering results in appearance of the electrons in the shower, which were absent in it before scattering, and in departure of the scattered positron from the shower, which is virtually tantamount to doubling of the excess electrons number. Both the positron and the electron when scattering at high energies retain the on-flying particle and the scattered one in the shower. Therefore one may not go beyond the calculation of the electron scattering by shower positrons, and double the result.

Cross-section of positrons differential as to the energy of  $\delta$ -electrons is represented by formula [7]:

$$\sigma_{\delta}(E_+, E)dE = \frac{2\pi_0^2 Z}{mc^2(\gamma_+^2 - 1)} \times \left[ \left( \frac{mc^2 \gamma_+}{E} \right)^2 - \frac{2\gamma_+^2 + 4\gamma_+ + 1}{\gamma_+ + 1} \cdot \frac{mc^2}{E} + \frac{3\gamma_+^2 + 6\gamma_+ + 4}{(\gamma_+ + 1)^2} \right] - \left[ \frac{2\gamma_+}{(\gamma_+ + 1)^2} \cdot \frac{E}{mc^2} + \left( \frac{E}{mc^2(\gamma_+ + 1)} \right)^2 \right] dE, \quad (10)$$

where  $\gamma_+ = (E_+ + mc^2)/(mc^2)$  – Lorenz-factor of the on-flying positron,  $E$  – kinetic energy of  $\delta$ -electron.

#### Ice (fresh water)

Differential energy spectrum of excess  $\delta$ -electrons in the shower maximum development is calculated by integrating all the positron energies exceeding the energy of the knocked-out  $\delta$ -electron:

$$N_{\delta}^{ice}(E)dE = 2 \cdot 0.5N_{max}n_{ice} \left\{ \int_{E_+=E}^{E_0} [2\sigma_{\delta}^H(E_+, E) + \sigma_{\delta}^O(E_+, E)] \Delta x_{ice} \varphi_e^{\max}(E_+) dE_+ \right\} dE. \quad (11)$$

In (11) all the symbols are analogous to those in (1), (3), (7), (10).

#### Air

$$N_{\delta}^{air}(E)dE = 2 \cdot 0.5Nn_{air} \left\{ \int_{E_+=E}^{E_0} \sigma_{\delta}^{air}(E_+, E) \Delta x_{air} \varphi_e^{\max}(E_+) dE_+ \right\} dE. \quad (12)$$

The symbols are the same as in formulas (1), (4), (8), (10).

#### Halite (NaCl)

$$N_{\delta}^{NaCl}(E)dE = 2 \cdot 0.5N_{max}n_{NaCl} \left\{ \int_{E_+=E}^{E_0} [\sigma_{\delta}^{Na}(E_+, E) + \sigma_{\delta}^{Cl}(E_+, E)] \Delta x_{NaCl} \varphi_e^{\max}(E_+) dE_+ \right\} dE. \quad (13)$$

The symbols are the same as in formulas (1), (3), (9), (10).

#### Compton electron excess caused by shower photon scattering on the medium electrons

Cross-section of the Compton scattering per one atom differential as to the scattered electron energy has the following form [7]:

$$\sigma_{comp}(E_\gamma, E)dE = \frac{\pi_0^2 Zmc^2}{E_\gamma^2} \left[ \frac{E_\gamma}{E_\gamma - E} + \frac{E_\gamma - E}{E_\gamma} + \left( \frac{mc^2}{E_\gamma - E} - \frac{mc^2}{E_\gamma} \right)^2 - 2mc^2 \left( \frac{1}{E_\gamma - E} - \frac{1}{E_\gamma} \right) \right] dE. \quad (14)$$

Here  $E_\gamma$  – energy of the shower photon, MeV.

#### Ice (fresh water)

Differential energy spectrum of the excess electrons in the shower maximum development is calculated by integrating all the shower photon energies exceeding a certain minimal energy  $E_\gamma^{\min}$  which is the function of the scattered electron energy. The Compton electron minimal energy  $E = 1$  MeV.

$$N_{comp}^{ice}(E)dE = N_{\max} n_{ice} \left\{ \int_{E_\gamma^{\min}}^{E_0} [2\sigma_{comp}^H(E_\gamma, E) + \sigma_{comp}^O(E_\gamma, E)] \Delta x_{ice} \varphi_\gamma^{\max}(E_\gamma) dE_\gamma \right\} dE. \quad (15)$$

Here  $E_\gamma^{\min} = 0.5(E + \sqrt{E^2 + 2mc^2E})$ , MeV;  $\Delta x_{ice} = 0.2/\mu_{ice}(E_\gamma)$  cm (1/5 of the average length of a photon free path) where  $\mu_{ice}(E_\gamma)$  is linear coefficient of  $\gamma$ -radiation intensity attenuation in the ice. The other values are described in (2), (3), (7), and (14).

#### Air

$$N_{comp}^{air}(E)dE = N n_{air} \left\{ \int_{E_\gamma^{\min}}^{E_0} \sigma_{comp}^{air}(E_\gamma, E) \Delta x_{air} \varphi_\gamma^{\max}(E_\gamma) dE_\gamma \right\} dE. \quad (16)$$

All the symbols are the same.  $\Delta x_{air} = 0.2/\mu_{air}(E_\gamma)$  cm, where  $\mu_{air}(E_\gamma)$  – linear coefficient of  $\gamma$ -radiation intensity attenuation in the air.

#### Halite (NaCl)

$$N_{comp}^{NaCl}(E)dE = N_{\max} n_{NaCl} \left\{ \int_{E_\gamma^{\min}}^{E_0} [\sigma_{comp}^{Na}(E_\gamma, E) + \sigma_{comp}^{Cl}(E_\gamma, E)] \Delta x_{NaCl} \varphi_\gamma^{\max}(E_\gamma) dE_\gamma \right\} dE. \quad (17)$$

The symbols are the same.  $\Delta x_{NaCl} = 0.2/\mu_{NaCl}(E_\gamma)$  cm, where  $\mu_{NaCl}(E_\gamma)$  – is linear coefficient of  $\gamma$ -radiation intensity attenuation in halite.

#### Total energy spectrum of the excess electrons in a shower or in EAS

Differential energy spectrum of the excess electrons summed up with all the considered effects taken into account and normalized to the total number of particles in the shower maximum development (ice, halite) or to the total number of EAS particles at the sea level (air) is:

$$F_{ex}(E)dE = \frac{N_{an}(E) + N_\delta(E) + N_{comp}(E)}{N_{\max}} dE \quad \text{or} \quad F_{ex}(E)dE = \frac{N_{an}(E) + N_\delta(E) + N_{comp}(E)}{N} dE. \quad (18)$$

In Fig. 1 spectra (18) for ice, air, and halite are shown. The steps in all the spectra are due to the minimal linear coefficient of  $\gamma$ -radiation intensity attenuation  $\mu_{\text{sub}}$  at energy  $E \approx 10$  MeV. Relative integral excess of shower electrons with energy  $E \geq 1$  MeV is  $\sim 23\%$  for ice,  $\sim 20\%$  for air, and  $\sim 15\%$  for halite. Integral excess for ice agrees well with the data obtained using Monte-Carlo method in [8]. At an arbitrary depth of the shower development in a condensed medium the spectrum (1) was transformed to the form:

$$\varphi_e(E)dE = \frac{2.29s}{E_{cr}} \cdot \frac{dE}{\left(1 + \frac{2.29}{E_{cr}}E\right)^{s+1}}, \quad (19)$$

where  $s$  – age parameter (see below). Accordingly, the spectrum (18) is roughly replaced by  $s \cdot F_{ex}(E)dE$ .

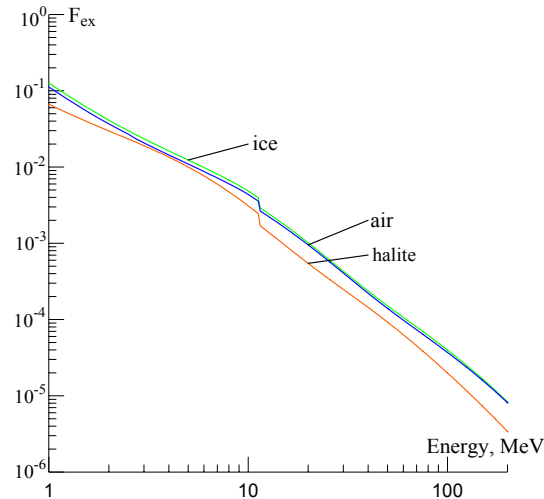


Fig.1. Differential energy spectra of the relative excess of shower electrons in ice, air, and halite. Integral relative electron excess at energy  $E \geq 1$  MeV in the shower maximum development makes 23%, 20% and 15%, accordingly.

### MAGNETIC INDUCTION OF ELECTRON-PHOTON AND EXTENSIVE AIR SHOWERS

A shower is a relativistically compressed, thin, azimuthally symmetrical disk formed of relativistic electrons, positrons and  $\gamma$ -quanta that is traveling in a medium with velocity virtually equal to that of light in vacuum. Radial, relative to the shower axis, distribution of charged particle number density (the number of particles referred to the unit area element) for the sake of simplicity is generally described as a Greisen approximation [9] for Nishimura and Kamata function [10,11]:

$$\rho(r, x) = \frac{0.443s^2(1.9-s)}{2\pi r_m^2} \left(\frac{r}{r_m}\right)^{s-2} \left(1 + \frac{r}{r_m}\right)^{s-4.5} N(x), \quad (20)$$

where  $r$  – is the distance between the particle and the shower axis,  $r_m = (E_s \cdot x_0) / (E_{cr} \cdot \rho_{sub})$  – is Moliere radius,  $E_s = 21$  MeV;  $x_0$  – radiation length in the matter where the shower is developed (for ice  $x_0 = 36.08$  g/cm<sup>2</sup>, for air  $x_0 = 37.1$  g/cm<sup>2</sup>, for halite  $x_0 = 22.2$  g/cm<sup>2</sup>;  $\rho_{sub}$  is the matter density g/cm<sup>3</sup>. Moliere radius  $r_m = 11.3$  cm for ice and  $r_m = 5.95$  cm for halite. The electron excess is supposed to have the same distribution in the shower as all the particles have. Cascade curve of the electron-photon shower [9] is:

$$N(x) = \frac{0.31}{\sqrt{\ln\left(\frac{E_0}{E_{cr}}\right)}} \exp\left[\left(\frac{x}{x_0}\right)(1 - 1.5 \ln(s))\right], \quad (21)$$

where  $x \geq 0$  – the matter present thickness;  $s = 3x / [x + 2x_0 \ln(E_0/E_{cr})]$  – age-parameter ( $N(x) = N_{max}$  – in its maximum (see formula (3)) for  $s=1$ ).

The EAS particle radial density at the sea level is often described by Greisen approximation for Nishimura and Kamata function, but with Linsly modifications [12]. For the EAS whose energy is higher than  $5 \cdot 10^{18}$  eV ( $N \geq 10^9$ )

$$\rho(r) = \frac{1.6}{2\pi r_m^2} \left(\frac{r}{r_m}\right)^{-1} \left(1 + \frac{r}{r_m}\right)^{-2.6} N, \quad (22)$$

and Moliere radius  $r_m = 78.9$  m. At lower energies the distribution (22) becomes more flat due to the second exponent decrease as to its absolute value, what is caused by EAS "aging".

In the medium at the distance  $R$  from the shower or the EAS the excess relativistic electron forms magnetic field  $H(t, R)$ , which is the function of the running time  $t$  common for all the particles [13] (see Fig.2):

$$H(t, R) = \frac{e\beta(1-\beta^2)\sin\theta}{L^2(1-\beta^2\sin^2\theta)^{3/2}}. \quad (23)$$

In this formula  $e$  – electron charge;  $\beta$  – ratio of the particle velocity to the velocity of light in vacuum;  $L = [(R^2 + r^2 - 2Rr\cos\varphi_r + [\beta c(t-\tau)]^2)^{1/2}]$  – the distance from the point of observation to the shower electron at the point of time  $t$ ;

$\sin \theta = \sqrt{1 - \left[ \frac{\beta c(t - \tau)}{L} \right]^2}$ ,  $\theta$  – the angle between the particle velocity direction and its electric field direction;

$\tau = \frac{n'}{c} \sqrt{R^2 + r^2 - 2rR \cos \varphi_r}$  – time of the electric and magnetic field spread in the medium from the shower particle to the point of observation, which coincided with the shower bunch plane;  $\varphi_r$  – azimuthal angle of the radius-vector  $r$  of an electron in the shower disk;  $n'$  – index of the sphere refraction in the radio-frequency range:  $n'_{ice} \approx 1.3$ ;  $n'_{NaCl} \approx 1.4$ ;  $n'_{air} = 1.00027 \approx 1^*$ .

Longitudinal relativistic current of the excess electrons produces magnetic induction in a medium at a distance R from the EAS axis (see Fig. 2).

$$B(t, R) = 10^{-4} \mu \int_{E_{min}}^{E_0} dE \int_0^{\infty} r dr \int_0^{2\pi} F_{ex}(E) \rho(r) H(t, R) \cos \alpha d\varphi_r, \tag{24}$$

where  $\mu$  – is relative magnetic permeability of the medium in which the magnetic induction is measured. It will be shown below that  $\mu$  should be chosen equal to 150. Functions  $F_{ex}(E)$ ,  $\rho(r)$  and  $H(t,R)$  that have been described in formulas (18), (22), and (23) were included in the subintegral expression. The projecting cosine  $\cos \alpha = (R - r \cos \varphi_r) / L$ , in which the angle  $\alpha$  is counted out between vector  $\vec{H}$  and the direction normal to the shower axis and the radius-vector  $\vec{R}$  of the point of observation. Magnetic field in (23) is calculated in gauss using CGSM system of units. Factor  $10^{-4}$  appears in (24) when we turn to SI-system. In media with radio-wave refraction index  $n > 1$  the magnetic field lags behind the field-generating particles, therefore it follows the shower to its axis under the Cerenkov angle.

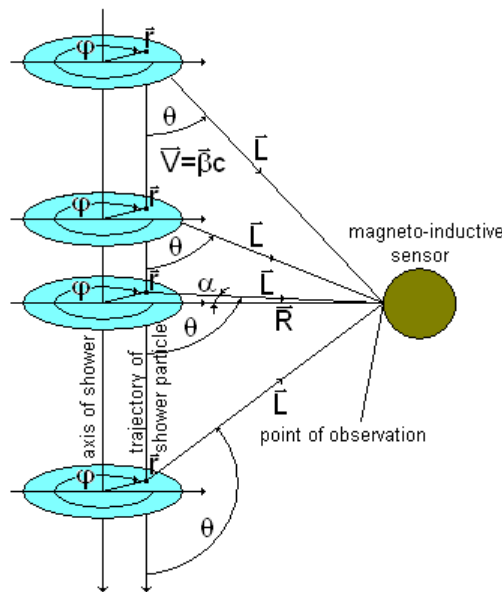


Fig.2. Geometric scheme of the shower magnetic induction formation at the point of observation. The symbols are described in the text.

Within the condensed media the path of the shower development and degradation is estimated to be several meters, therefore the expression (24) will be changed.  $s(x)$  (age parameter) and  $\rho(r,x)$  (shower particle density) should be inserted under the integral sign, and  $x$  should be expressed as a function of the running time  $t$  (see formulas (20) and (21)):

$$B(t, R) = 10^{-4} \mu \int_{E_{min}}^{E_0} dE \int_0^{\infty} r dr \int_0^{2\pi} s(t) F_{ex}(E) \rho(r, t) H(t, R) \cos \alpha d\varphi_r, \tag{25}$$

$x = x_0 \ln(E_0/E_{cr}) + \beta c(t - \tau)$ . Here  $x$  and  $x_0$  are assumed to be measured in centimeters. Since a shower starts at  $x=0$ , then minimal time  $t_{min}$  at any values of  $\tau$  should not yield negative  $x$ .

\* After completing this calculations the authors specified the values of refraction indices within the radio-frequency range:  $\langle n'_{ice} \rangle = 1.775$ ,  $\langle n'_{NaCl} \rangle = 2.366$ ,  $\langle n'_{air} \rangle = 1.00034$  (with water vapor influence taking into account). The calculation results for the value and shape of the output magnetic induction pulses will be corrected in the process of preparation to real experiments.

Figures 3 and 4 summarize the calculation results on magnetic induction of electron-photon showers in ice and halite, as well as that of extensive air showers in air as functions of time and distance from their axis, based on formulas (24) and (25). The pulse amplitude of the magnetic induction is quite predictable to decrease in inverse proportion to the squared distance (see (23)) with increasing the pulse duration. In condensed media the pulse duration for long distances is limited by the time of the shower development and absorption, and its shape roughly replicates that of the cascade curve as the time function  $t$ .

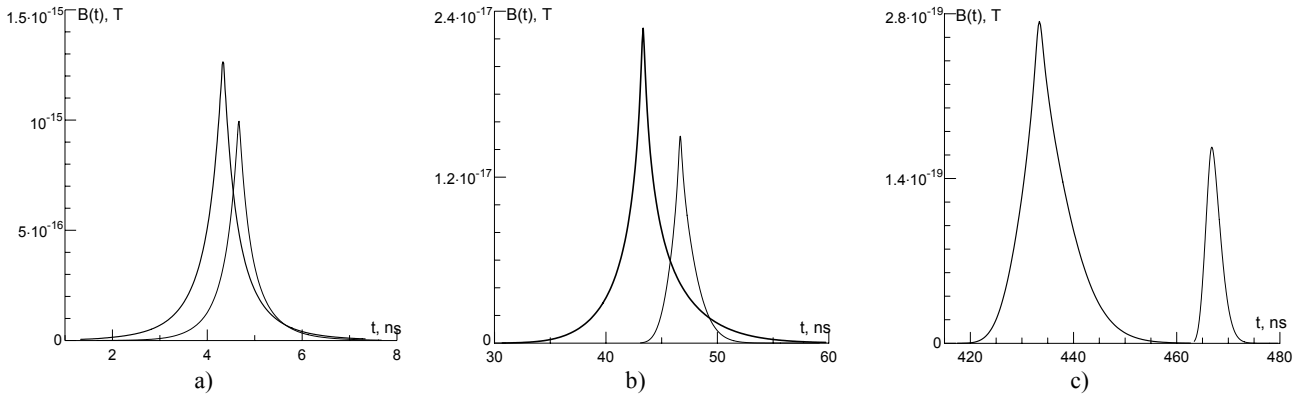


Fig.3. Magnetic induction per one particle in the maximum of the electron-photon shower  $B(t)$  in ice (bold curve), and in halite at different distances.

a)  $R=1\text{m}$ , b)  $R=10\text{ m}$ , c)  $R=100\text{ m}$ .  $B(t)$  was calculated in teslas (T),  $t$  – in nanoseconds (ns),  $\mu=150$ .

Now a certain technical device should be chosen to efficiently detect the shower magnetic induction.

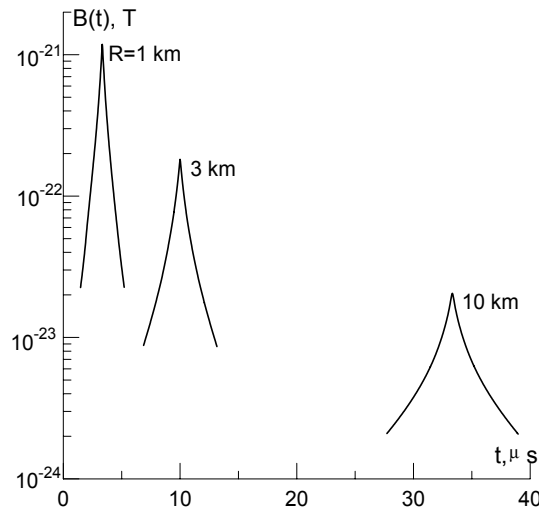


Fig. 4. Magnetic induction per one particle in extensive air showers  $B(t)$  at the sea level at different distances.

$B(t)$  is calculated in teslas (T),  $t$  – in microseconds ( $\mu\text{s}$ ),  $\mu=150$ .

### DETECTOR OF SHOWER MAGNETIC INDUCTION

A coaxial cable coil in the form of a circle is used as a magnetic induction detector. For simplicity sake the detector area  $S$  may be assumed to be  $1\text{ m}^2$ . The outer cable conductor should be cut half way around in order to avoid short circuit electric currents running through it and, hence, compensation of the currents running through the inner conductor. It will serve as an electric shield for the inner conductor. It is advisable to use a miniature coaxial cable with wave resistance  $\rho_0=50\text{ Ohm}$ . To amplify the shower magnetic induction the coil area should be filled with a high-frequency thermostable ferromagnetic material. M-metal type 150-HF nickel-zinc ferrites, whose relative magnetic permeability  $\mu=130\div 170$  does not change up to 20 MHz, may answer these demands to some extent. The tiny cable is put down into a slot at the edge of the ferrite plate. Technological feasibility to manufacture a plate of such a large area has not been considered yet. The coaxial cable loop forms a sneak parallel oscillatory-circuit with a resonant frequency.

$$f_{\text{res}} = \frac{1}{2\pi\rho_0 C\sqrt{\mu}}, \quad (26)$$

where  $l$ ,  $\rho_0$ ,  $C$  – are, accordingly, length, wave resistance, and linear capacity of the cable section. The product of  $\rho_0 C=5\cdot 10^{-9}\text{ Ohm}\cdot\text{F}$  for conventional coaxial cables. Assuming  $l\approx 3.55\text{ m}$  ( $S=1\text{ m}^2$ ),  $\mu=150$  in equation (26) we will have  $f_{\text{res}}=7.32\cdot 10^5\text{ Hz}$ . To make the detector pass-band wider one should use a band-pass filter of a ladder type [14], with the detector parasitic oscillatory-circuit serving as an input component. A version of the detector is shown in Fig. 5. The

filter parameters are as follows:  $\rho_1 = \rho_0 \mu^{1/2} = 612 \text{ Ohm}$ ; lower cut-off frequency  $f_{-1} = 25 \text{ kHz}$ , upper cut-off frequency  $f_{+1} = 21.44 \text{ MHz}$ ,  $\Delta f = f_{+1} - f_{-1} = 21.44 \text{ MHz}$ ,  $C_1 = C_4 = 355 \text{ pF}$ ,  $L_1 = L_4 = 133 \text{ }\mu\text{H}$ ,  $C_2 = 532 \text{ pF}$ ,  $L_2 = 88,8 \text{ }\mu\text{H}$ ,  $C_3 = 0.61 \text{ }\mu\text{F}$ ,  $L_3 = 0.0778 \text{ }\mu\text{H}$ . The authors calculated and measured minutely the real frequency response of this filter, but in order to simplify further calculations they assumed it to be ideal.

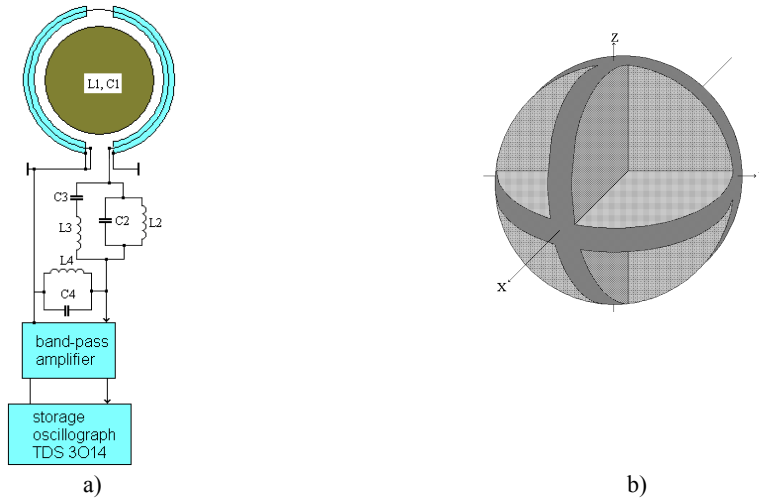


Fig. 5. The shower magnetic induction detector.

a) Block diagram of the detector. The detector space was filled with a high-frequency thermostable ferrite having relative magnetic permeability  $\mu = 150$ . b) Possible configuration of the ferrite infill for three-coordinated system of magnetic induction detectors.

**MAGNETIC INDUCTION FLOW ACROSS THE DETECTOR AREA**

Let us place the detector in the plane formed by the shower axis and the observation-point radius-vector  $R$ . The magnetic flow across the detector area does not cover it straight away, but moves over it in the longitudinal and radial directions. Therefore it constitutes composition of the magnetic induction and the detector area component variable in time:

$$\Phi(t, R) = \frac{2c^2}{n'^2} \int_{t-t_0}^t B(t, R) \sqrt{\frac{n'd}{c}(t-t') - (t-t')^2} dt', \tag{27}$$

where  $d = 2(S/\pi)^{1/2} = 2/\pi^{1/2}$  – is the detector diameter ( $S = 1 \text{ m}^2$ ),  $t' \leq t$ ,  $t_0 = (n'd)/c$  – maximum time of the magnetic induction motion over the detector area,  $n'$  – refraction index of the medium where the shower develops. The results of the calculations made using formula (27) for the showers in ice and halite are summarized in Fig. 6. EAS magnetic flow at long distances, expressed in webers, numerically coincided with magnetic induction (see Fig. 4), therefore its graphic chart has not been shown.

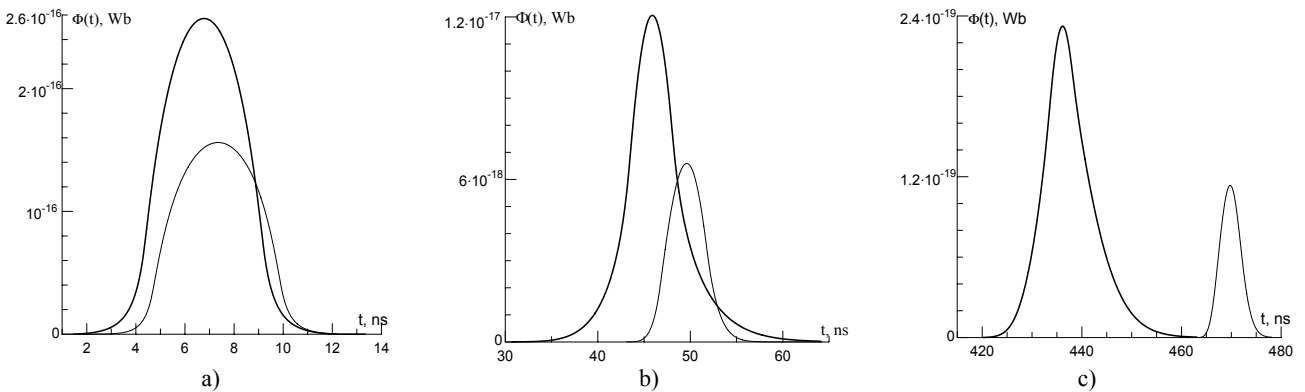


Fig. 6. Magnetic induction flow per one particle in the electron-photon shower maximum  $F(t)$  in ice (bold line), and in halite at different distances.

a)  $R = 1 \text{ m}$ , b)  $R = 10 \text{ m}$ , c)  $R = 100 \text{ m}$ .  $F(t)$  was calculated in webers (Wb),  $t$  – in nanoseconds (ns),  $\mu = 150$ .

**MAGNETOINDUCTIVE SHOWER PULSES ARISING AT THE DETECTOR INPUT AND THE FILTER OUTPUT**

Electromotive force (EMF) of the electromagnetic induction  $U_{in}(t, R)$  at the filter input was calculated by formula:

$$U_{in}(t, R) = - \frac{d\Phi(t, R)}{dt} \tag{28}$$

and was measured in volts (V). The results of EMF calculations by formula (28) for showers in condensed media are shown in Fig.7.

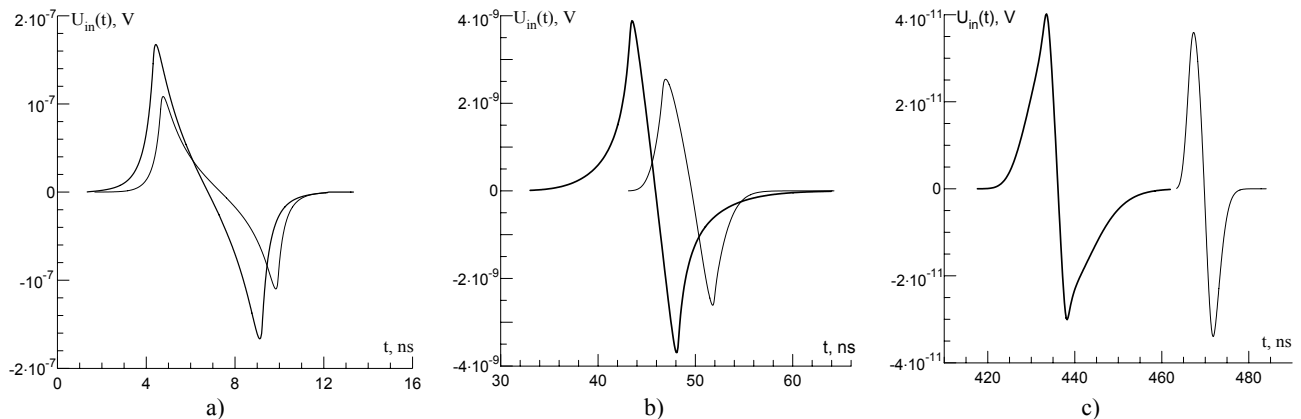


Fig. 7. Magnetoinductive pulses per one particle in shower maximum in ice (bold lines), and in halite at the filter input at different distances. a)  $R=1$  m, b)  $R=10$  m, c)  $R=100$  m.  $\mu=150$ .

Magnetoinductive pulse at the detector output is the evaluation result of convolution of the incoming pulse and the normalized pulse-response of the band-pass filter  $h(t)$ :

$$U_{out}(t, R) = \int_0^t U_{in}(t', R) h(t-t') dt'. \quad (29)$$

Here  $h(t) = \frac{\sin[\pi(f_{+1} - f_{-1})t]}{t} \cos[\pi(f_{+1} + f_{-1})t]$ , the normality condition:  $\int_{-\infty}^{\infty} h(t) dt = 1$  and  $t' \leq t$ , as the signal at the output cannot pass ahead the signal at the filter input.

Fig. 8 shows the magnitude and shape of the magnetoinductive pulses at the output of the detector of the showers that have reached their maximum in condensed media (according to (29)).

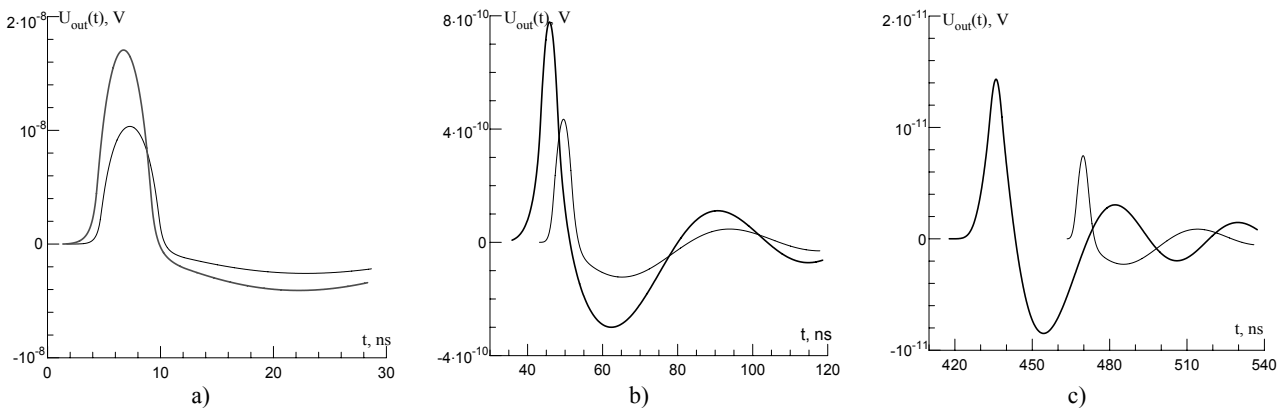


Fig. 8. Magnetoinductive pulses for one particle in shower-maximum in ice (bold curves), and in halite at the filter output (Fig. 5) at different distances. a)  $R=1$  m, b)  $R=10$  m, c)  $R=100$  m.  $\mu=150$ .

In Fig. 9 input and output magnetoinductive pulses caused by EAS and recorded by the same detector are shown.

It should be noted that the described method has restrictions for small distances, both in condensed media, and in air. In condensed media the detector considerable dimensions, comparable to radial distance from the axis of the shower, cause indeterminacy due to strong diversion of the magnetic induction magnitude and shape as a function of time within the detector overall dimensions. In air the Moliere radius is long ( $r_m=78.9$  m), and the detector, which has appeared inside a shower, will add up magnetic fields of various directions, including mutually antithetical. This will also cause distortion of the function radial distribution of the output signal amplitude at small distances. Therefore, when showers are detected in condensed media, minimum detection distances should exceed overall dimensions of the detector several times, and for EAS –  $R > (2 \div 3) r_m$ .

To increase sensitivity of the EAS magnetic detector (Fig.5) at considerable distances one should use the Manganese-zinc ferrites such as 2000MN3 with higher thermal stability. Their working frequency range lays in the interval  $f=0 \div 1$  MHz. In this case the filter parameters will be: relative magnetic conductivity  $\mu=2000$ ,  $f_{-1}=40$  kHz,  $f_{+1}=1$  MHz,  $\Delta f=f_{+1}-f_{-1}=0,96$  MHz,  $\rho_1=\rho_0 \sqrt{\mu}=2,236$  k $\Omega$ ,  $f_{res}=0,2$  MHz,  $C1=C4=355$  pF,  $L1=L4=397$   $\mu$ H,  $C2=53,2$  pF,  $L2=1,19$   $\mu$ H,  $C3=1,636 \cdot 10^4$  pF,  $L3=38,7$   $\mu$ H.

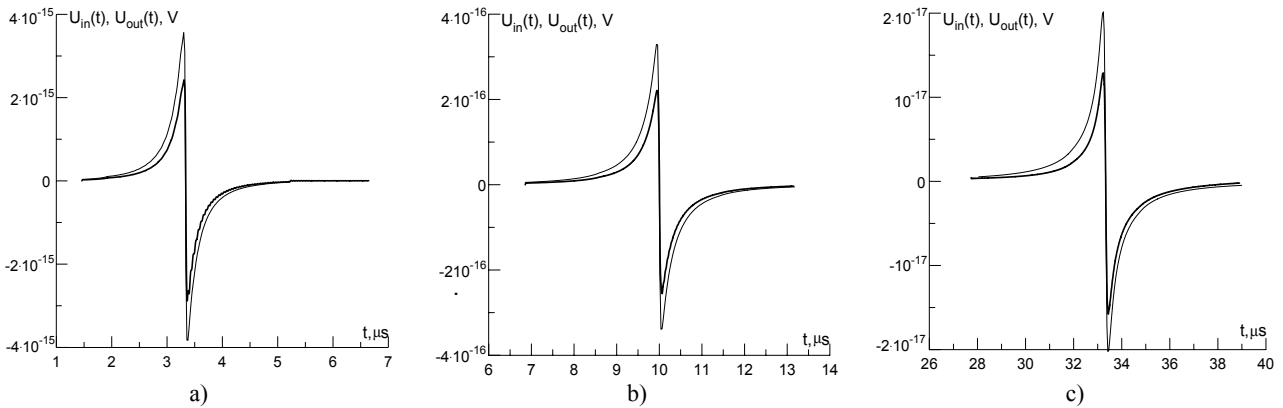


Fig. 9. Magnetoinductive pulses per one particle of EAS at the detector input and output (bold curves). The distance from the point of observation to EAS axis  $R=1$  km (a), 3 km (b), 10 km (c),  $\mu=150$ .

Epures of magnetoinductive pulses at the output of the filter with the above-mentioned performances are shown in Fig. 10.

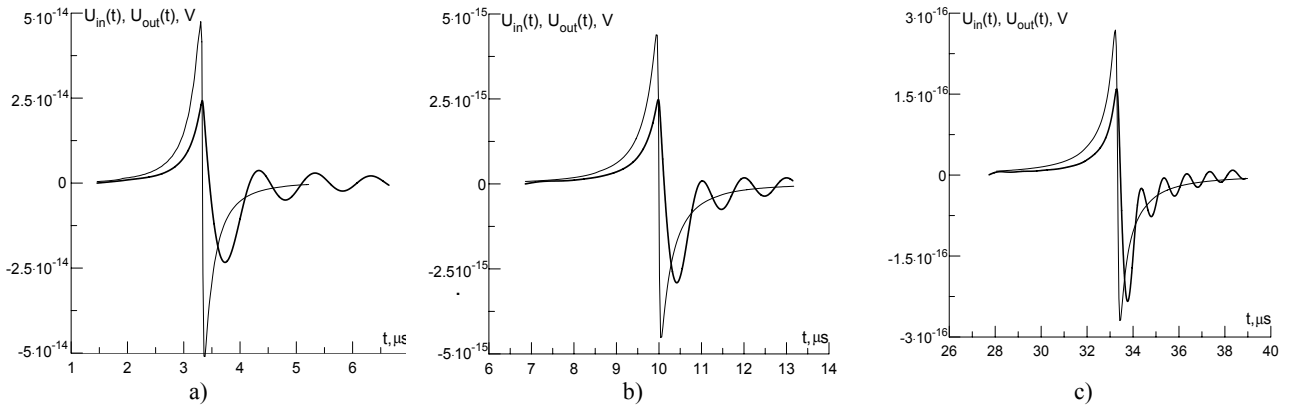


Fig.10. Magnetoinductive pulses per one particle of EAS at the magnetic detector input and output (bold curves). The distance between the observation point and the EAS axis  $R=1$  km (a), 3 km (b), 10 km (c).  $\mu=2000$ .

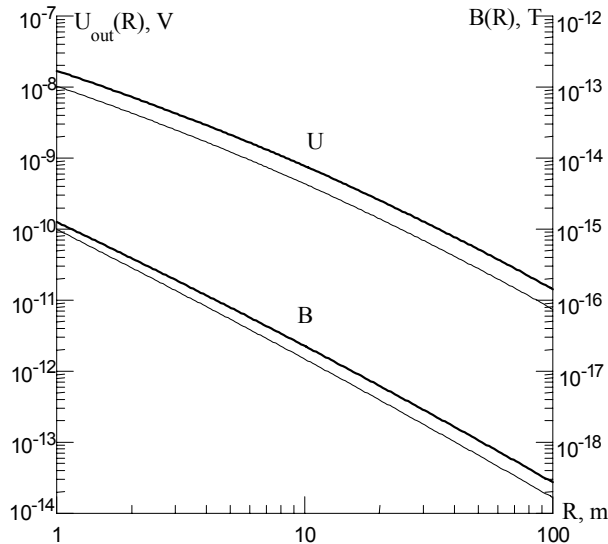


Fig.11. Radial distribution of magnetic induction normalized for one particle in the shower maximum and corresponding amplitudes of the output magnetoinductive pulse of showers in ice (bold curves) and halite,  $\mu=150$ .

As the result of all evaluations, in Fig. 11 and 12 radial distributions of amplitudes of the magnetic induction and the output induction pulses of showers, accordingly, in condensed media and in air are given. Using them one can evaluate the energy threshold for the neutrinos detected in thick strata of ice or halite ( $E_{\gamma} \sim 10^{12}$  eV) and the galaxy cosmic charged particles ( $E_0 \sim 10^{16}$  eV).

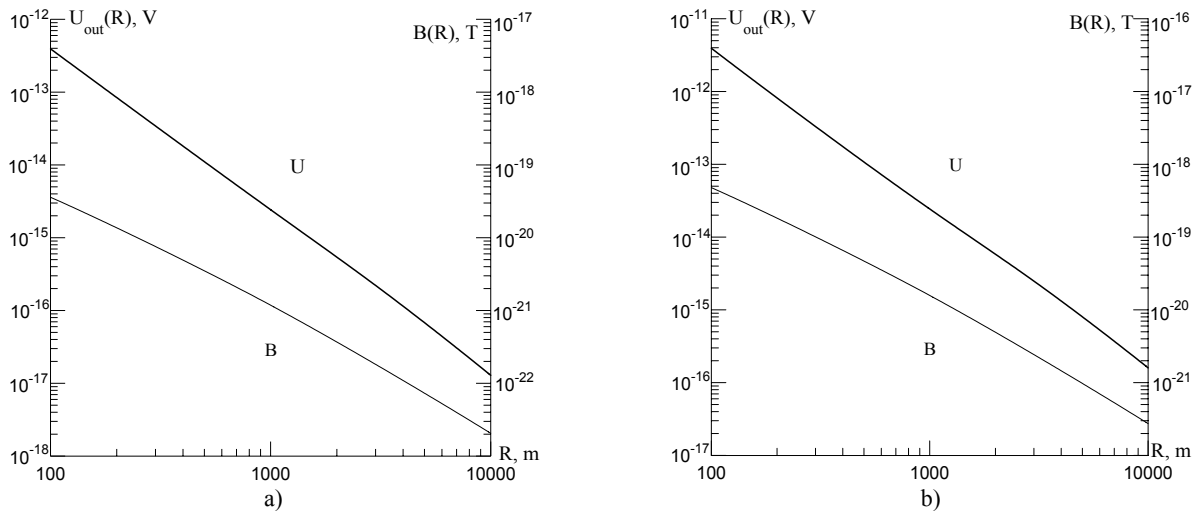


Fig. 12. Radial distribution of magnetic induction normalized for one particle at the sea level and corresponding amplitude of the output magnetoinductive pulses of EAS for  $\mu=150$  (a), and  $\mu=2000$  (b).

### CONCLUSION

The calculations of the magnetoinductive effect similar to those demonstrated above were performed with the assistance of the authors earlier as well, although they were not so comprehensive [5, 15-17]. Every time they were stimulated by putting into operation of large-scale experimental EAS detecting facilities such as Yakut device and AKENO (AGASA), or by such outstanding projects as EAS-1000, PIERRE AUGER. The experiments with neutrinos performed in Baikal lake (ND-200) and in the Antarctica ice stratums (AMANDA) became an analogous incentive for the authors. We have known about some independent works of some other authors in which magnetoinductive effect was evaluated and a technique of its detection, different from that described above, was proposed [18, 19].

Possible applications of the magnetoinductive method were considered by the authors earlier [5, 17]. First of all, it was an examination of the initial power spectrum of cosmic rays in the range of relict truncating energy [20, 21]. It is possible to manufacture a system of induction detectors, with the effective range of EAS detection up to 300 sq. km. For this purpose, it is necessary to arrange three detectors in three mutually perpendicular (vertical and horizontal) planes at one point of observation. Then, the total amplitude of their output pulses  $U_{out}(R) = \sqrt{(U_{out})_x^2 + (U_{out})_y^2 + (U_{out})_z^2}$ , where indexes x, y, z were for the pulse amplitudes defined by the detectors versus magnetic induction projections to the coordinate axes, would not depend on the direction of EAS arrival. But, at the same time, the direction cosines of EAS axis would be defined. By the least estimations, productivity of the combined detector in registering EAS with energy  $E_0 > 4 \cdot 10^{19}$  eV ( $N > 10^{10}$ ) is likely to be 3÷4 events per year. The system comprising three detectors does not require a lot of place and can be located in a region proof from anthropogenic electrical and magnetic disturbances, for example, on top of a predominant mountain. In this case the solid angle of detectors would increase almost twice and can attain  $\pi$  sr, what would give the same increase of productivity in EAS detection. But here selection of EAS and fixation of the instant of its arrival should be done using two charged particle detectors of considerable dimensions connected to the coincidence circuit, and located in immediate proximity from the system of detectors. A principal shortage of such an application of the magnetoinductive method is a serious error in definition of the EAS arrival instant owing to the considerable curvature of its front and growth of its width at the circumference. Application of considerable number of detecting magnetic systems is much more favorable.

Promising (but not unique) territory for the arrangement of systems of magnetic induction detectors is Antarctica. Despite severe climatic conditions, conducting of experiment in Antarctica has advantages due to lack of thunderstorms, industrial radio noises, and its vast not populated territory. Mounting the above mentioned systems of magnetic detectors with a local entry of the information at the distance of ~5 km from one another, it is possible to provide as much of effective area of EAS detection as you like. As long as  $U_{out}(R) = \xi N/R^2$  (see Fig. 12), where  $\xi$  – a dimension factor of proportionality, one can do without application of detectors of charged particles. Distance R between the observation point and the EAS axis was proportional to the induction pulse delay time relative to the moment of the particle bunch central part passing through the plane in which radius-vector R (see Fig. 2) was situated. Uniform time scale for all self-sufficient systems of magnetic detectors at given accuracy ~10 nanoseconds ensures precise enough measurement of value R. For this purpose the induction signal arrival at not less than two observation points is necessary. Factor  $\xi$  for the magnetic detectors to be used was computed and then checked and refined in the process of preliminary tests on one of the operating EAS detecting facilities. The number of particles in EAS was determined at known  $U_{out}(R)$ ,  $\xi$  and R.

In the same place, in Antarctica, deep in ice, vertical chains of analogous systems of magnetic detectors can detect

neutrinos of ultrahigh energies, and such an experiment under the title AMANDA, but with application of traditional optical Cerenkov method, has already been under implementation [22]. The distance between the chains was determined by the energy threshold of the detected showers (see Fig. 11). Polarity of the registered signals would depend on the global direction of neutrino arrival (from the upper or lower hemispheres).

Halite-fields also may serve as a natural target for interactions among cosmic neutrinos of super-high energies. Just such a halite-field is Solotvin salt-mine (Transcarpathian region, Ukraine) whose cupola volume is more than  $1 \text{ km}^3$  [23]. The cupola top part together with the layer of pebbles and marl with thickness of about 34 meters is at a height of 283.7 meters above the sea level, and its base is at a great depth (more than 1 km). The layer of pebbles shields fairly well the volume filled with halite from the outside high-frequency electric disturbances, thus maintaining rather high sensibility of recording apparatus. Therefore, the Solotvin field would be rather promising for arranging the systems of magnetic induction detectors at its area. Most likely, it is not an unique example of a salt-mine of this kind in the terrestrial globe. As, for example, the Artemovsk field that is also in Ukraine.

#### REFERENCES

1. Askarjan G.A. *Surplus negative charge of electron-photon shower and its coherent radio emission.* // *JETP.* – 1961. – V. 41. – P. 616 – 618. (Rus.)
2. Tamm Ig., Belenky S. // *J. Phys. USSR.* – 1939. – V. 1. – P. 177.
3. Belenky S.Z. *Avalanche processes in cosmic rays,* Moscow, Leningrad, 1948. – 244 p. (Rus.)
4. Zatsepin V.I., Chudakov A.E. *Spatial distribution of Cerenkov light from extensive air showers.* // *JETP.* – 1962. – V. 42. – P. 1622 – 1628. (Rus.)
5. Zalyubovskii I.I., Kartashev V.M., Kovtun V.E., Minko O.K., Shmatko E.S. *Magnetoinductive effect of electron-photon showers developed in thick ice stratums.* // *Radiophysics and Radio Astronomy.* – 2002. – V. 7, N 3. – P. 254 – 264. (Rus.)
6. D'yakonov M.N., Egorov T.A., Efimov N.N., Pravdin M.I., Sleptsov I.E. *Cosmic radiation of extremely high energy,* Novosibirsk: Nauka, Siberia Division, 1991. – 251 p. (Rus.)
7. Akhiezer A.I., Berestetskii V.B. *Quantum Electrodynamics,* Moscow, 1969. – 624 p. (Rus.)
8. Zas E., Halzen F., Stanev T. // *Phys. Rev. D.* – 1992. – V. 45, N1. – P. 362 – 375.
9. Greisen K. *Extensive air showers.* In book: *Physics of cosmic rays.* Ed. by J. Vilson, Moscow, 1958. – V. 3. – P. 7 – 141. (Rus.)
10. Nishimura J., Kamata K. // *Progr. Theor. Phys.* – 1950. – V. 5. – P. 899.
11. Nishimura J., Kamata K. // *Progr. Theor. Phys.* – 1951. – V. 6. – P. 628.
12. Linsley J. *Proc. 8<sup>th</sup> Int. Cosmic Rays Conf.* Jaipur, 1963. – V. 4. – P. 77 – 99.
13. Landau L.D., Lifshits E.M. *Field theory,* Moscow, 1988. – 510 p. (Chapter V, § 38, p. 128-130). (Rus.)
14. Sakharova T.M. *Calculation of frequency responses of electric filter working attenuation,* Moscow, 1968. – 327 p. (Rus.)
15. Shmatko E.S. *Spectral distribution of EAS radio emission.* Thesis of Candidate of science in physics and mathematics. Kharkov, 1978, 121 p. (Rus.)
16. Shmatko E.S., Molotko S.P., Kartashev V.M., Lazarev A.V., Dudnik A.V. *Inductive effect of extensive air showers.* // *Problems of Nuclear Physics and Cosmic Rays. Kharkov, KSU,* 1988, N30. – P. 3-11. (Rus.)
17. Kartashev V.M., Kovtun V.E., Shmatko E.S. *Magnetoinductive technique for detecting extensive air showers with maximum high energies.* // *Radiophysics and Radio Astronomy.* – 1999. – V. 4, N 1. – P. 61 – 68. (Rus.)
18. Golubnichii P.I., Philonenko A.D., Tsarev V.A. *Electromagnetic detection of extensive air showers.* // *Izvestiya of USSR Academy of Science, Physical series.* – 1991. – V. 55, N4. – P. 727-729. (Rus.)
19. Philonenko A.D., *Cascade shower radio emission and detection of cosmic rays with super-high energy.* Lugansk, 2002. – 280 p. (Section 1.10.1, p. 62-66). (Rus.)
20. Greisen K. // *Phys. Rev Lett.* – 1966. – V. 16. – P. 748 – 750.
21. Zatsepin G.T., Kuzmin V.A. // *Pis'ma v ZETP.* – 1966. – V. 4. – P. 78 – 79. (Rus.)
22. Andres E., Askebjerg P., Barvik S. et al. // *Nucl. Phys. B (Proc. Suppl.).* – 1999. – V. 75A. – P. 412.
23. Zdesenko Yu.G., Kropivnyanskii B.N., Kuts V.N., et al. *Study of backgrounds for scintillation and semiconductor detectors at an underground low-background laboratory of the INR, Ukrainian Academy of Science.* Preprint, KINR-85-28. Kiev, 1985. (Rus.)

#### ВОЗМОЖНОСТЬ ДЕТЕКТИРОВАНИЯ КОСМИЧЕСКИХ ЧАСТИЦ И НЕЙТРИНО СВЕРХВЫСОКИХ ЭНЕРГИЙ В АТМОСФЕРНОМ ВОЗДУХЕ И КОНДЕНСИРОВАННЫХ СРЕДАХ МАГНИТОИНДУКЦИОННЫМ МЕТОДОМ

В.М. Карташев, В.Е. Ковтун, О.К. Минко, Ю.П. Полторацкая, Е.С. Шматко, И.И. Залюбовский

Харьковский национальный университет им. В.Н. Каразина, Харьков, Украина

Рассмотрена возможность детектирования космических частиц и нейтрино сверхвысоких энергий на основе электромагнитной индукции электронного избытка в широком атмосферном ливне (ШАЛ) и в ливнях в конденсированных средах (лёд, галит). Произведен расчёт электромагнитной индукции от ливней в указанных средах. Предложена конструкция детектора, основанного на данном принципе. Рассчитан отклик детектора на различных расстояниях от оси ливня. Оценен энергетический порог детектора, составляющий  $\sim 10^{12}$  эВ для ливней в конденсированных средах и  $\sim 10^{16}$  эВ для ШАЛ.

**КЛЮЧЕВЫЕ СЛОВА:** широкий атмосферный ливень, электронный избыток, электромагнитная индукция ливня, индукционный детектор.